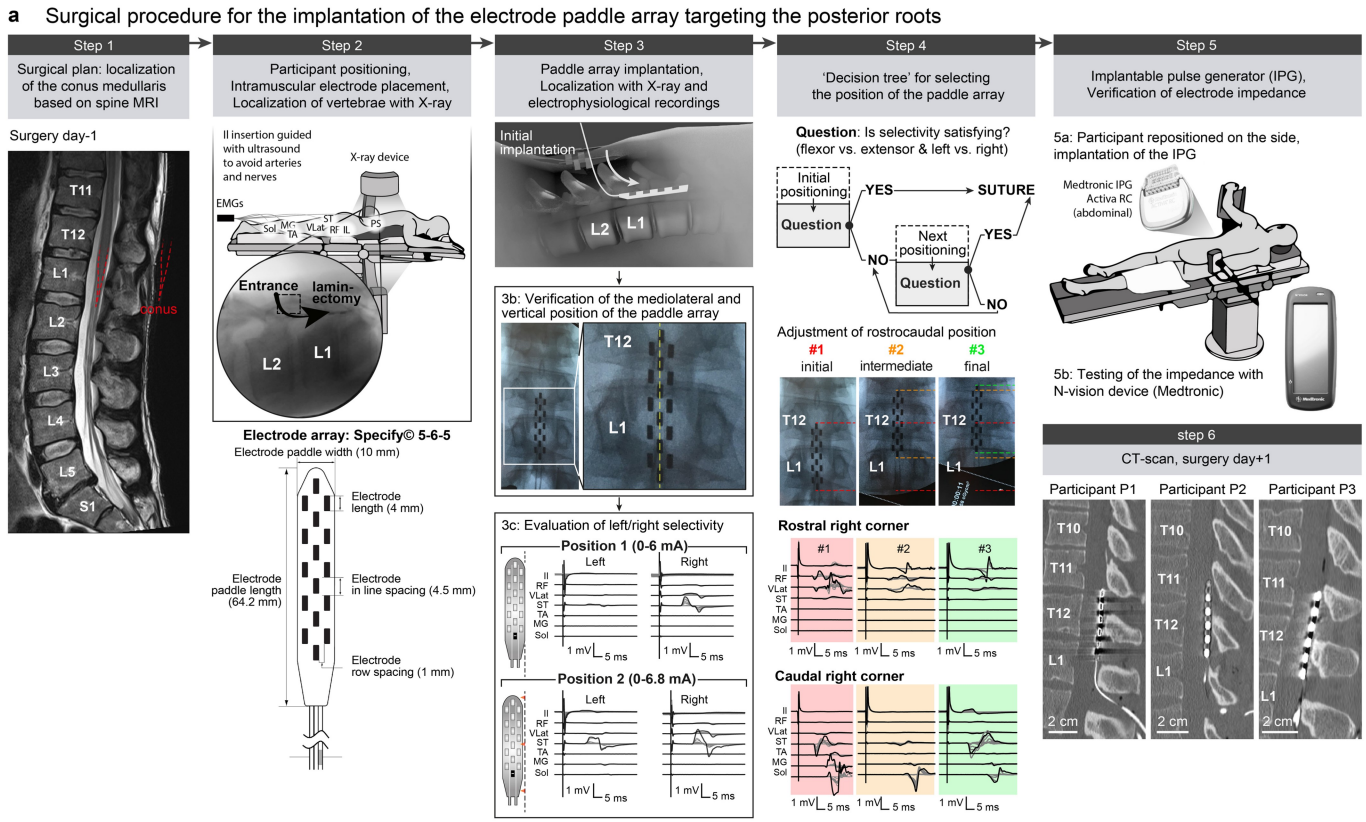

Extended Data Fig. 1 | Surgical procedure and technological framework. a, Surgery. Step 1: high-resolution MRI for pre-surgical planning. The entry point into the epidural space is based on the position of the conus. Step 2: placement of subdermal and intramuscular needle EMG electrodes for key leg muscles and paraspinal (PS) muscles. A subdermal needle is inserted over the sacrum and used as a return electrode for stimulation. Bottom, schematic of the 16-electrode paddle array. Step 3: surgical openings based on pre-surgical planning, typically between the L1 and L2 vertebrae, which are identified through intraoperative X-ray. The mediolateral positions of the paddle array are evaluated with X-ray and recordings of EMG responses following single pulses of EES delivered to the most rostral or most caudal midline electrodes. Step 4: the rostrocaudal position of the paddle array is optimized using EMG responses to single-pulse EES delivered to the electrodes located at each corner of the paddle array. The aim is to obtain strong ipsilateral responses in hip flexors with the most rostral electrodes and strong ipsilateral responses in ankle extensors with the most caudal electrodes. Step 5: implantable pulse generator (IPG) placed within the abdomen. Once connected to the paddle array, the impedance of the electrodes is evaluated to verify that all the components are properly connected. Step 6: post-surgical CT scan showing the location of the paddle array with respect to the vertebrae in each participant. **b**, Technological framework and surgical procedure. Step 1: participants wear reflective markers that are monitored using infrared cameras. An algorithm assigns the markers to the joints in real-time. Step 2: the spatiotemporal trajectory of the foot around a calculated centre of rotation (centroid, updated every 3 s) is converted into angular coordinates that trigger and terminate EES protocols when a user-defined threshold is crossed. Step 3: EES commands are transmitted to the IPG via Bluetooth (1) to a module that converts them into infrared signals (2), which are then transferred to the stimulation programmer device (2′). Step 4: the stimulation programmer transmits EES commands into the IPG (4) via induction telemetry, using an antenna (3) taped to the skin and aligned to the IPG. EES is delivered through the paddle array (5).

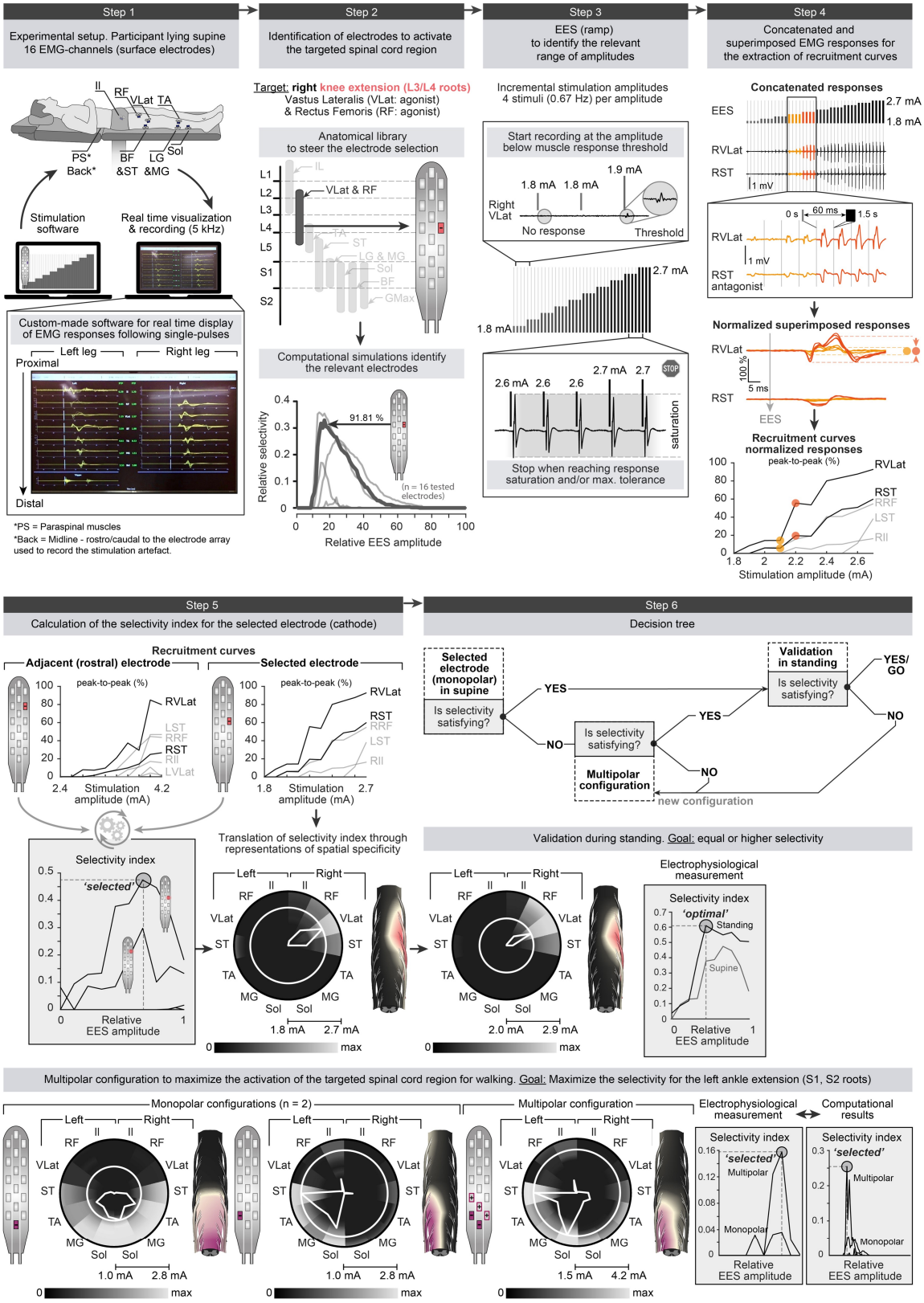

Extended Data Fig. 2 | See next page for caption.

Extended Data Fig. 2 | Identification of electrode configurations to target selected posterior roots. Step 1: single-pulse EES and EMG recording setup. Step 2: motor neuron pools are located in specific segments, which provides information on the relative recruitment of each posterior root with EES. For example, electrodes targeting the L3 or L4 posterior roots will elicit the strongest EMG responses in the knee extensors. A personalized computational model of EES allows the performance of simulations that evaluate the relative activation of a given posterior root with a given electrode over the entire amplitude range. Each curve corresponds to an electrode. The highlighted curve corresponds to the electrode selected after steps 3–5. Step 3: single pulses of EES are delivered through the subset of electrodes identified by simulations. The EMG responses are recorded over a broad range of EES amplitudes. Step 4: the EMG responses are concatenated and averaged across $n = 4$ repetitions for each EMG amplitude, and the peak-to-peak amplitude of the average responses is calculated to elaborate a recruitment curve for each recorded leg muscle (black traces: targeted muscles). Step 5: the circular plots display the normalized EMG responses (greyscale) when delivering single-pulse EES at increasing amplitudes (radial axis), where the white circle highlights the optimal EES amplitude and the polygon quantifies the relative muscular selectivity at this amplitude (median response taken over $n = 4$ EES pulses). The motor neuron activation maps are shown for the optimal amplitudes. Step 6: decision tree to validate or optimize electrode configurations. The selected electrode is tested during standing as the position of the spinal cord with respect to the paddle array can change between supine and standing. In this example, the selectivity improves during standing. When the selectivity is deemed insufficient, the current is steered towards the targeted posterior roots using multipolar configurations. The example shows the increased selectivity of a multipolar configuration with two cathodes surrounded by three anodes, compared to the two corresponding monopolar configurations. These results were verified experimentally and with computer simulations.

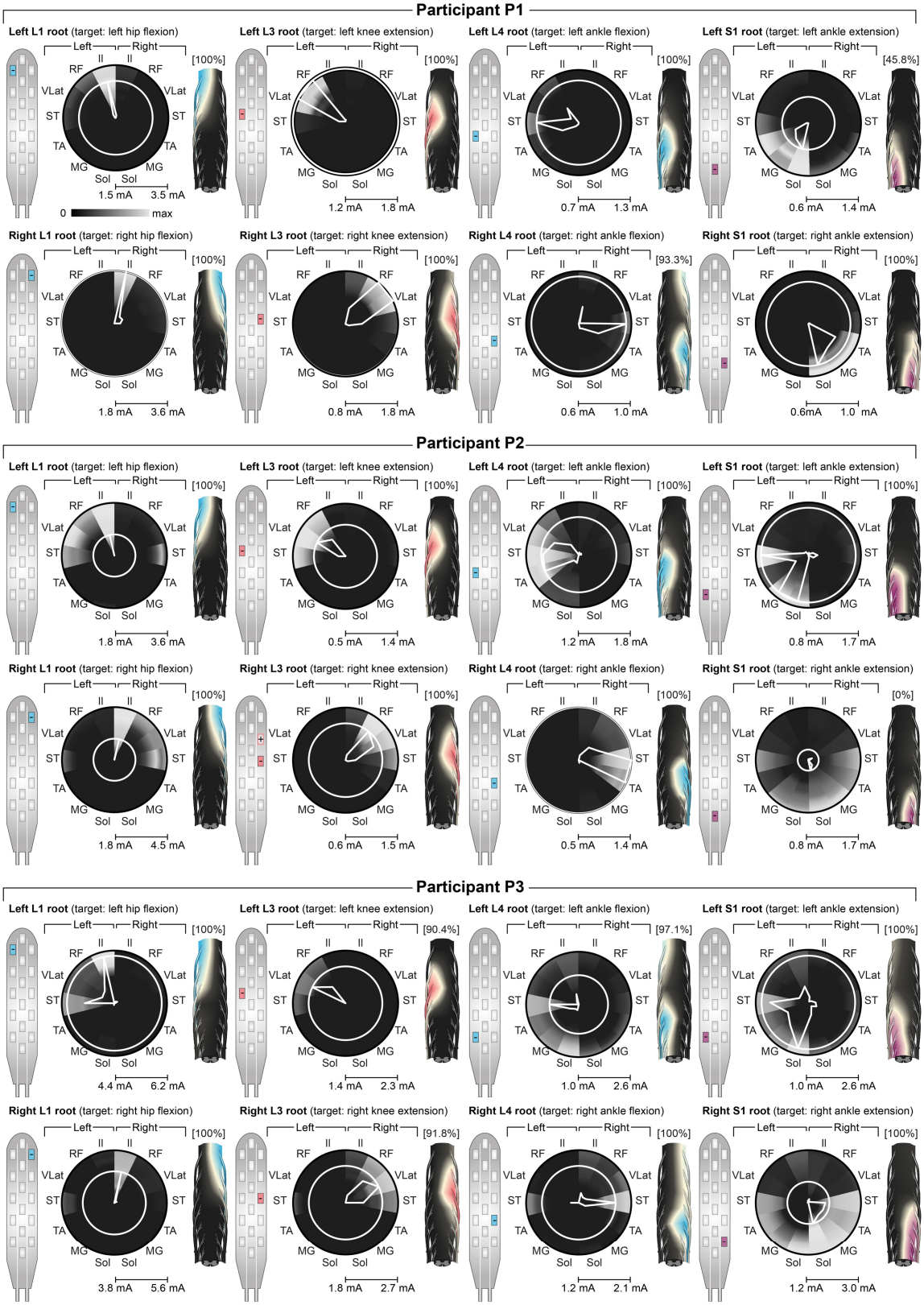

Extended Data Fig. 3 | Spatial selectivity of targeted electrode configurations. Monopolar configurations (shown on paddle array schematics) experimentally selected to target the left and right posterior roots associated with hip flexion (L1), knee extension (L3), ankle flexion (L4) and ankle extension (S1) for the three participants. The circular plots and motor neuron activation maps use the same conventions as in Fig. 2 and Extended Data Fig. 2 (median of $n = 4$ pulses). The normalized selectivity index is reported above each motor neuron activation map. This index represents the percentage of posterior root selectivity for the electrode configuration selected experimentally, with respect to the maximum posterior root selectivity that can be achieved among all monopolar configurations (all selectivity indices obtained from computational simulations). Note that in P2, the electrode selected experimentally to target the right S1 root was located on the midline and resulted in bilateral activation within computational simulations, which resulted in a normalized selectivity index of zero.

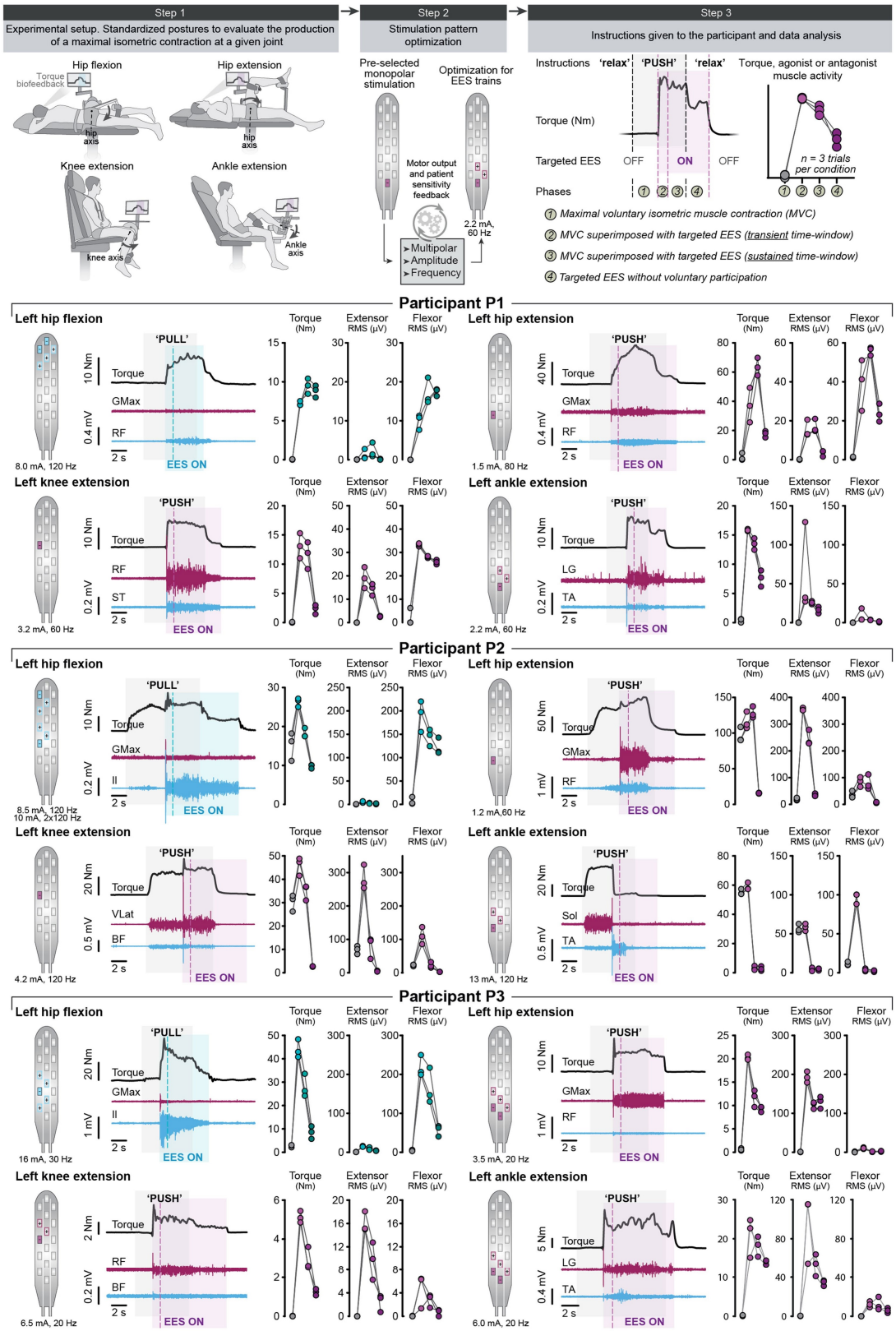

Extended Data Fig. 4 | See next page for caption.

Extended Data Fig. 4 | Single-joint movements enabled by targeted EES. Step 1: participants are placed in standardized positions to allow assessment of voluntary torque production at a single joint (isometric contractions) without and with targeted EES. Step 2: EES protocols elaborated from single-pulse experiments (Extended Data Figs. 2, 3) are optimized for each task using multipolar configurations and adjustments of EES amplitude and frequency. Step 3: sequence of each trial. Participants were asked to produce a maximal voluntary contribution, but failed in most cases, as evidenced by the absence of EMG activity during this period. While they continued trying to activate the targeted muscle, EES was switched on. After a few seconds, participants were instructed to stop their voluntary contribution. After a short delay, EES was switched off. For each sequence, the produced torque and EMG activity of the key agonist and antagonist muscles acting at the targeted joint were calculated over the four indicated phases of the trial. Plots report the measured torques and EMG activity during the various phase of the trial for the left legs of all participants for the four tested joints (cyan, flexor; magenta, extensor), together with EES parameters and electrode configurations. All measurements were performed before rehabilitation, except for hip extension in P1 and P2 (not tested before), and ankle extension in P3 (no capacity before rehabilitation), which were carried out after rehabilitation. Targeted EES enabled or augmented the specific recruitment of the targeted muscle, which resulted in the production of the desired torque at the targeted joint, except for ankle extension of P2. Plots show quantification of the EMG activity and torque for $n = 3$ trials per condition. Note that hip flexion can be enabled or augmented with EES targeting L1 and/or L4 posterior roots (heteronymous facilitation of flexor motor neuron pools).

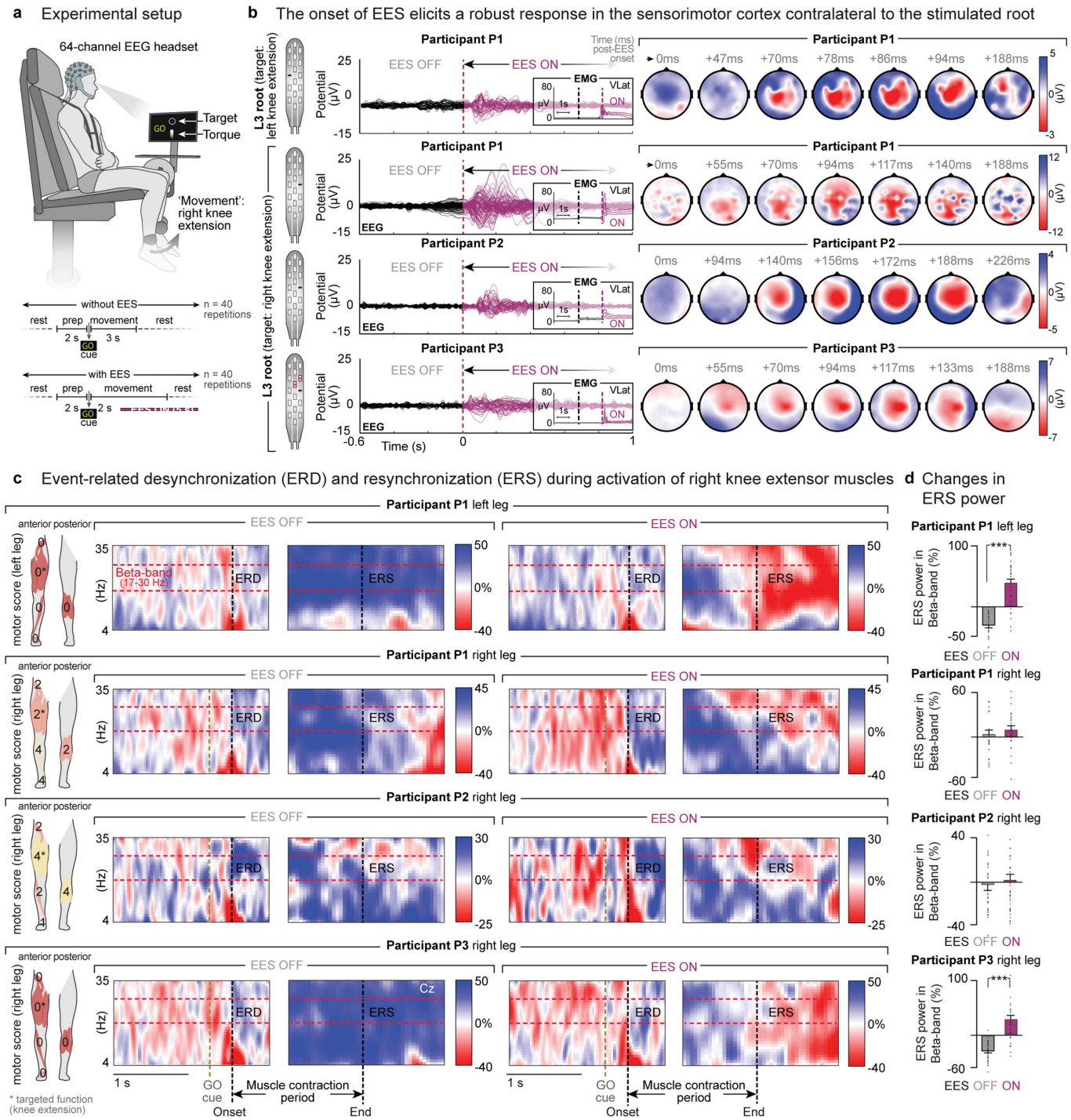

Extended Data Fig. 5 | Modulation of EEG activity during volitional contraction of leg muscles without and with EES. a, Recordings of EEG activity while participants were asked to produce an isometric torque at the knee joint without and with continuous EES targeting motor neuron pools innervating knee extensors, as shown in **b**. **b**, Superimposed EEG responses ($n = 40$ repetitions) and temporal changes in the topography of average activity over the cortical surface after the onset of EES, as indicated above each map. The onset was calculated from the onset of EMG responses in the targeted vastus lateralis muscle (insets). The stimulation elicited a robust event-related response over the left sensorimotor cortex with a latency of 90 ± 40 ms for P1 and P3, and of 170 ± 40 ms for P2 (full range of the peaks and middle of this range indicated). **c**, Average normalized time–frequency plots ($n = 40$ trials) showing ERD and ERS over the Cz electrode (central top electrode) for each individual during the voluntary activation of knee extensor muscles without and with EES. Schematic drawings (left) indicate the motor scores of the tested legs, including the targeted muscles (*), at the time of enrolment in the study. Both legs were tested in P1 owing to his asymmetric deficits. **d**, Normalized average power (mean ± s.e.m.) of the β-band over the Cz electrode during ERS from 0 to 500 ms after termination of contraction without and with continuous EES ($n = 40$ repetitions for each condition, individual data points shown except for outliers more than 3 median absolute deviations away from the median). ***$P < 0.001$ (permutation tests, see Methods).

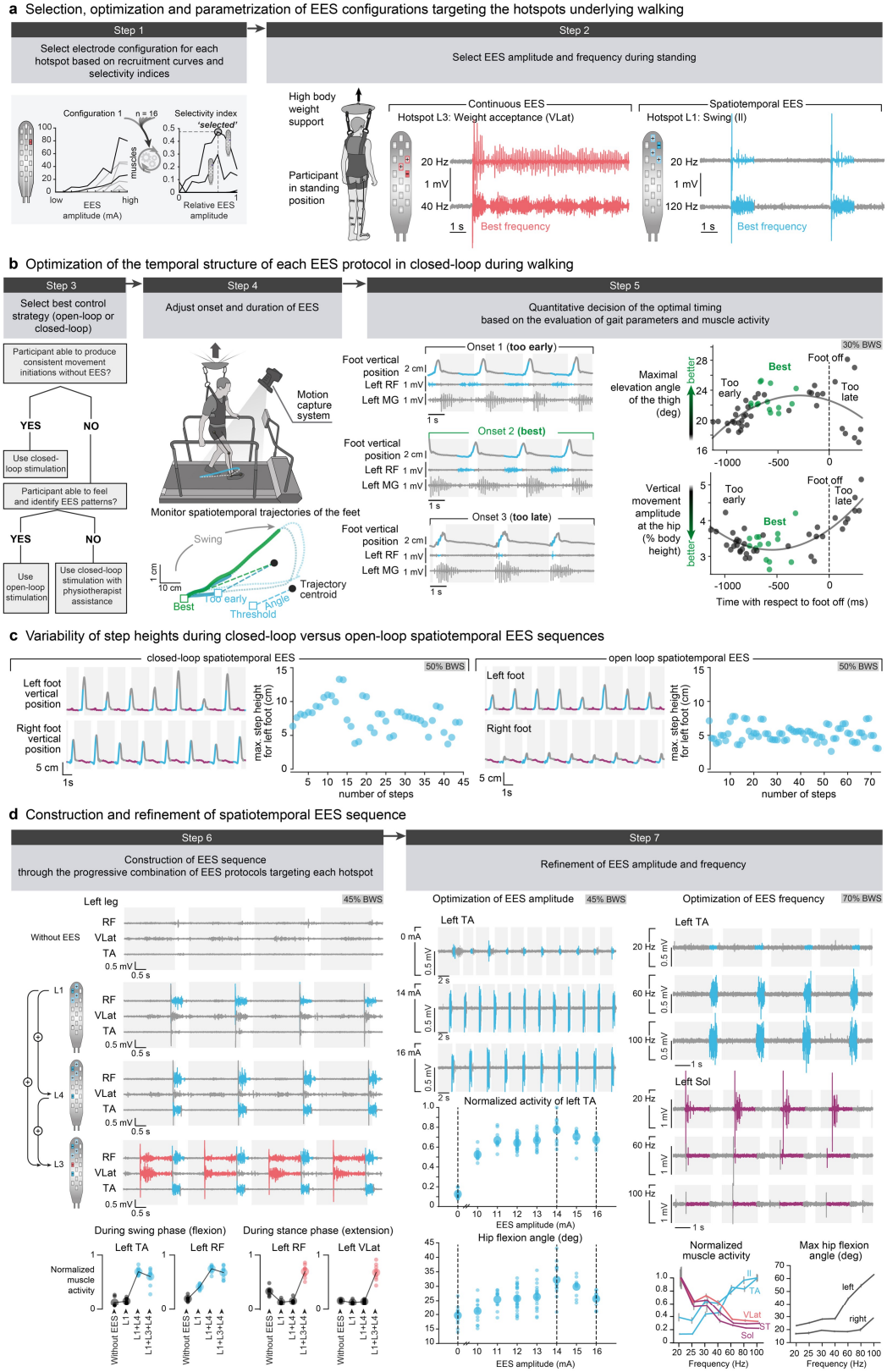

Extended Data Fig. 6 | See next page for caption.

Extended Data Fig. 6 | Configuration of spatiotemporal EES to enable walking. a, Spatial configuration. Step 1: select electrode configurations from single-pulse experiments to target the three hotspots underlying the production of walking in healthy individuals (weight acceptance: L3; propulsion: S1; swing: L1/L4). Step 2: optimize EES amplitude and frequency while delivering EES during standing. Multipolar configurations can be used to refine selectivity of EES protocols. Example shows continuous EES targeting the right L3 posterior root to facilitate right knee extension during standing, and trains (500 ms) of EES targeting the right L1 posterior root stimulation to facilitate hip flexion. Two EES frequencies are shown (P3). **b**, Temporal configuration. Step 3: decision tree to select the best strategy to configure the temporal structure of EES protocols. If the participant is able to initiate leg movements consistently, use closed-loop EES based on real-time processing of foot trajectory. If the participant is not able to initiate consistent leg movements but can feel when EES is applied, use open-loop EES. If the participant is not able to generate movement and cannot feel EES, use closed-loop EES combined with physiotherapist assistance to move the legs. Step 4: real-time monitoring of the spatiotemporal trajectory of the feet. The trajectory is modelled as a foot rotating in space around the centroid of the movement (updated every 3 s). Angular thresholds determine the onset and end of EES protocols. Step 5: example showing the effect of three different angular thresholds on the onset of EES and resulting kinematics and EMG activity, including the quantification of kinematics for each step and condition that enables selecting the optimal onset of EES trains (P1). The same approach is used to optimize the duration of each train. **c**, Comparisons between closed-loop and open-loop EES. Plots show the vertical displacements of the left and right feet and successive step heights during walking with spatiotemporal EES delivered in closed loop versus open loop, showing the reduced variability of step height during pre-programmed EES sequences (P1). **d**, Resulting EMG patterns. Step 6: example of the progressive addition of EES protocols targeting specific hotspots. Plots show the quantification of EMG activity for the displayed muscles ($n = 7$ gait cycles for no EES and $n = 9$ gait cycles for each stimulation condition, P2). Step 7: EES amplitudes and frequencies are adjusted to avoid detrimental interactions between the different EES protocols and thus obtain the desired kinematic and EMG activity. Plots report the modulation of EMG activity and kinematics with increases in EES amplitude and frequency (mean ± s.e.m.; amplitude data: $n = 10, 12, 12, 30, 19, 12, 11, 10$ gait cycles for amplitudes in increasing order, P2; frequency data: $n = 20, 15, 16, 17, 15, 16, 15$ gait cycles for frequencies in increasing order, P3).

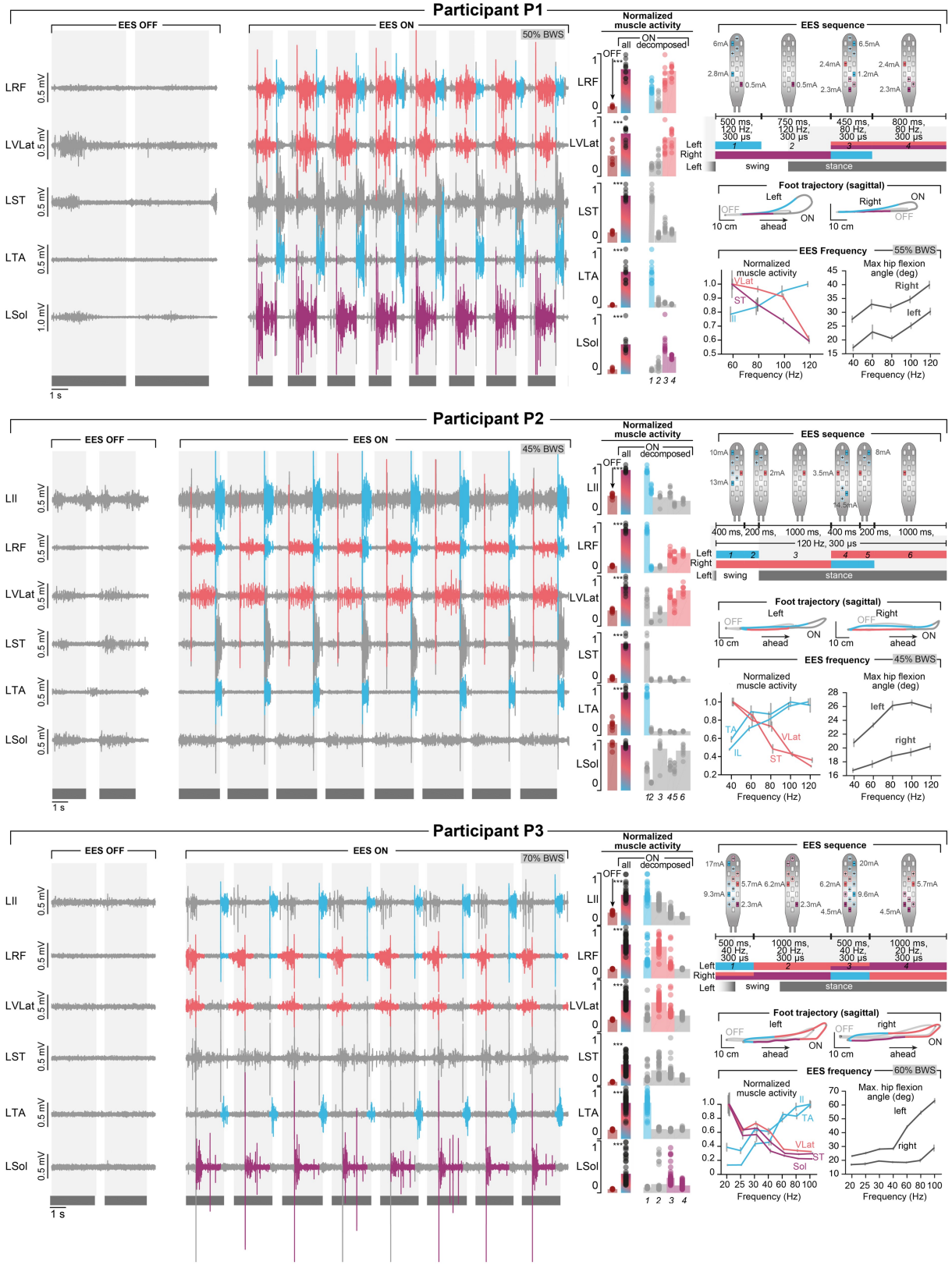

Extended Data Fig. 7 | See next page for caption.

Extended Data Fig. 7 | Targeted modulation of muscle activity during walking. Each panel reports the same representative data and quantification for one participant. Left, EMG activity of leg muscles during walking on a treadmill without EES (EES OFF) and with spatiotemporal EES (EES ON) while applying 50%, 45% and 70% body weight support for participants P1, P2 and P3, respectively. Stance and swing phases are indicated by grey and white backgrounds, respectively. The personalized spatiotemporal EES sequence (open loop) is schematized at the top right. The colours of each EES protocol refer to the targeted hotspots: weight acceptance (salmon), propulsion (magenta) and swing (cyan). These colours are used in the EMG traces to indicate the temporal window over which each targeted EES protocol is active. The bar plots report the amplitude of muscle activity without EES and with spatiotemporal EES, for which the quantification was performed over the entire burst of EMG activity and during each temporal window with targeted EES. The temporal windows are labelled with a number that refers to the spatiotemporal EES sequence. These results show the pronounced increase in the EMG activity of the targeted muscles (P1, no EES: $n = 7$ gait cycles, EES: $n = 11$ gait cycles; P2, no EES: $n = 9$ gait cycles, EES: $n = 9$ gait cycles; P3, no EES: $n = 10$ gait cycles, EES: $n = 57$ gait cycles). The average spatiotemporal trajectories of both feet with respect to the hip in the sagittal plane are shown for walking without EES and with spatiotemporal EES. The presence of targeted EES is indicated with the same colour code. Plots at bottom right show the relationships between EES frequency and the modulation of the EMG activity of flexor (blue) and extensor (magenta or salmon) muscles and maximum amplitude of hip movements during walking (mean ± s.e.m.; P1: $n = 14, 17, 15, 19$ gait cycles for increasing frequencies; P2: $n = 13, 16, 10, 17, 12$ gait cycles for increasing frequencies; P3: $n = 20, 15, 16, 17, 15, 16, 15$ gait cycles for increasing frequencies). $^{***}P < 0.001$. Student's t-test.

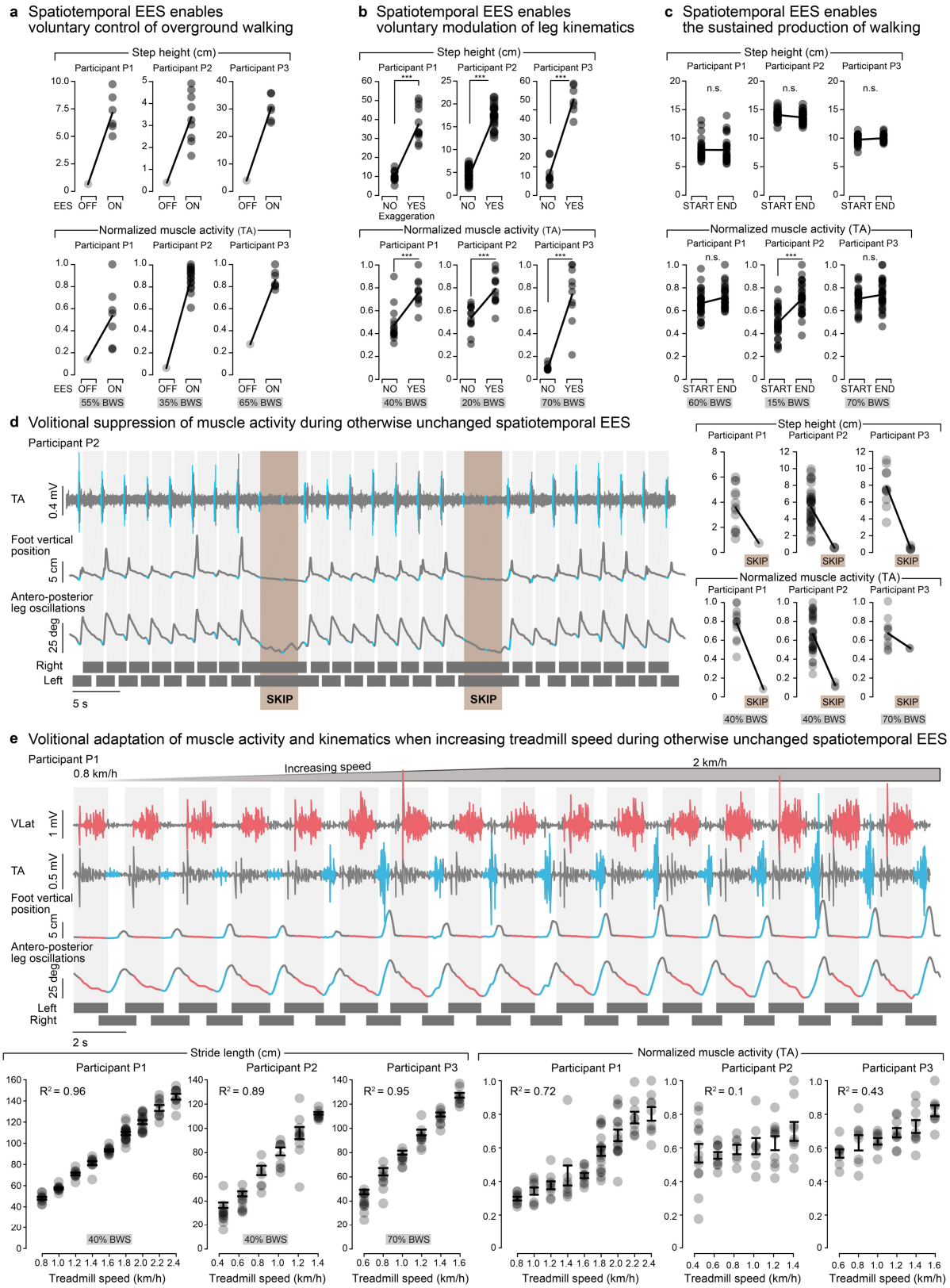

Extended Data Fig. 8 | See next page for caption.

Extended Data Fig. 8 | Volitional adaptations of walking during otherwise unchanged spatiotemporal EES. a–c, Quantifications of experiments shown in Fig. 4a–c for each participant. **a**, Step height and TA EMG activity with and without EES during overground walking (P1, EES ON: $n = 7$ gait cycles; P2, EES ON: $n = 16$ gait cycles; P3, EES ON, $n = 7$ gait cycles). **b**, Step height and TA EMG activity during normal steps and when participants were requested to perform exaggerated step elevations during overground walking (P1, $n = 15$ normal gait cycles, $n = 11$ exaggerated gait cycles; P2, $n = 31$ normal gait cycles, $n = 23$ exaggerated gait cycles; P3, $n = 14$ normal gait cycles, $n = 10$ exaggerated gait cycles). **c**, Step height and TA EMG activity during the first and last 30 steps extracted from a sequence of 1 h of locomotion on a treadmill ($n = 30$ gait cycles for all conditions). $^{***}P < 0.001$; n.s., non-significant; Student's *t*-test. **d**, EMG activity of representative leg muscles, vertical displacements of the foot and anteroposterior oscillations of the leg (virtual limb joining the hip to the foot) while P2 was walking continuously on the treadmill with spatiotemporal EES (open loop). The participant was asked to suppress the effects of EES and stand during one cycle of open-loop spatiotemporal EES sequence, highlighted in brown (SKIP), whereas he actively contributed to the production of movement the rest of the time. Plots report the quantification of step height and TA EMG activity during walking and when skipping steps for each participant (P1, $n = 13$ normal gait cycles, $n = 1$ skipped cycles; P2, $n = 36$ normal gait cycles, $n = 3$ skipped gait cycles; P3, $n = 11$ normal gait cycles, $n = 2$ skipped cycles). **e**, EMG activity of two representative muscles, vertical displacements of the foot and anteroposterior oscillations of the leg while P1 was walking on the treadmill and the speed of the belt increased progressively from 0.8 to 2 km h^{-1}. Plots show relationships between treadmill speed and mean stride length and TA EMG activity in all participants (P1: $n = 9, 9, 9, 9, 10, 18, 15, 9, 9$ gait cycles for increasing speeds; P2: $n = 13, 10, 7, 8, 10, 9$ gait cycles for increasing speeds; P3: $n = 8, 8, 10, 9, 9, 8$ gait cycles for increasing speeds; s.e.m. shown). The range of tested speeds was adapted to the walking ability of each participant.